Single-particle and multiparticle analysis of nucleus-nucleus collisions at 14.6, 60, and 200 GeV/nucleon

H. von Gersdorff, J. Amundson, P. S. Freier, J. Kapusta, and C. J. Waddington
School of Physics and Astronomy, University of Minnesota, Minneapolis, Minnesota 55455

L. M. Barbier, W. V. Jones, K. H. Moon, I. G. Park, O. E. Pruet, and J. P. Wefel
Department of Physics and Astronomy, Louisiana State University, Baton Rouge, Louisiana 70803

R. Holynski, A. Jurak, A. Olszewski, M. Szarska, B. Wilczynska, H. Wilczynski, W. Wolter, B. Wosiek, and K. Wozniak
Institute of Nuclear Physics, Krakow, Poland

(Received 16 November 1988)

The angles of all charged secondaries have been measured in central collisions of ^{16}O with AgBr at 14.6, 60, and 200 GeV per nucleon. The pseudorapidity distributions are approximately Gaussian in shape. The widths increase monotonically with beam energy, but are essentially independent of multiplicity at a fixed beam energy. Quantitatively, the widths are consistent with Landau's hydrodynamical model and inconsistent with a spherical fireball model and with Bjorken's hydrodynamical scaling model. There are no statistically significant correlations in the azimuthal angle of the observed charged secondaries. Analysis of the two-particle pseudorapidity correlation functions and of the pseudorapidity gap distributions provide no evidence of significant cluster production. The data are consistent with a Monte Carlo simulation based on independent emission of the secondary particles, although intrinsic few-particle correlations could be hidden by the high multiplicities in these events.

I. INTRODUCTION

The recent acceleration of ^{16}O nuclei to 14.6 GeV per nucleon at Brookhaven National Laboratory (BNL) and to 60 and 200 GeV per nucleon at CERN, and the subsequent detection of secondaries coming from collisions of the beam nuclei with various heavy target nuclei by many groups, has greatly advanced the experimental study of ultrarelativistic nucleus-nucleus collisions.[1] Central collisions with up to 300 charged particles for ^{16}O+AgBr at 200A GeV,[2] pseudorapidity densities of up to 140 charged particles per unit rapidity in ^{16}O+Ag interactions,[3,4] and transverse energies (E_T) as high as 150 GeV in the pseudorapidity range $-0.1<\eta<2.9$ for ^{16}O+Ag at 200A GeV,[5,6] have been observed. The target nuclei were found to completely disintegrate into light particles with $Z<3$ in the wake of the ^{16}O projectile.[7] Underlying the experiments is the search for evidence that the hadronic matter in these violent collisions made a transition, temporarily, to a deconfined quark-gluon plasma.

In a previous paper[2] the KLM collaboration presented its first results (experiments E808 at BNL and EMU07 at CERN) on the multiplicity and pseudorapidity distributions of ^{16}O+AgBr at the three aforementioned energies. Since then more events have been studied, and in this paper we use the current ^{16}O data set.

Details on the KLM emulsions and multiplicity analysis may be found in Ref. 2. For the purpose of this paper the essential facts are as follows. An emulsion is used as the AgBr target and as a 4π detector at the same time. The tracks left by essentially all charged particles emerging from the collision can be seen and their angles relative to the projectile direction measured by microscope. These angles are then transformed to pseudorapidities η [see Eq. (1)], which have typically errors $\Delta\eta=0.02$ and 0.08 for $\eta=1$ and 5, respectively. Charged secondaries, which are all we discuss in this paper, are particles of charge ±1, with ionization $\leq 1.4I_{\min}$ (minimum ionizing). We have analyzed only those events with the number of heavily ionizing (ionization $>1.4I_{\min}$) particles $N_h>15$. This removes all components of the emulsion other than Ag and Br as targets for the interactions studied here. It also serves as a central trigger, eliminating peripheral interactions of the ^{16}O with AgBr. These central collisions represent (17±2)% of the total inelastic cross section and (31±3)% of the interactions with Ag and Br. Charged secondaries consist, for the most part, of pions with laboratory kinetic energy greater than 70 MeV. There are also some kaons with kinetic energy greater than 250 MeV and some protons with kinetic energy greater than 400 MeV. Unfortunately, it is extremely difficult, at our energies, to separate charged secondaries into protons, kaons and pions and to measure their mean transverse momentum $\langle p_T\rangle$; we have not attempted to do so here, though this has been done before for cosmic-ray events.[8]

Given the advantages and limitations of emulsion, we proceed to analyze the data in the following way. In Sec. II we present the full pseudorapidity distributions at 14.6A, 60A, and 200A GeV. In Sec. III we study the az-

imuthal asymmetry correlation as a function of pseudorapidity. In Sec. IV we present the two-particle pseudorapidity correlation function at the three energies. In Sec. V we present results on the n-gap pseudorapidity distribution, which is designed to find cluster formations. Finally, in Sec. VI, we summarize and present our conclusions based on these data.

II. PSEUDORAPIDITY DISTRIBUTIONS

The single-particle pseudorapidity distribution is one of the fundamental distributions in high-energy collisions. Although it is a one-body distribution which integrates over all correlations, nevertheless it can provide us with important information about the dynamics of the collisions, as we shall see.

Recall the definition of pseudorapidity η, which is not Lorentz invariant,

$$\eta=\tfrac{1}{2}\ln\left[\frac{p+p_z}{p-p_z}\right]=\tfrac{1}{2}\ln\left[\frac{1+\cos\theta}{1-\cos\theta}\right]$$
$$=-\ln\tan(\theta/2)\ , \tag{1}$$

where p_z and θ are the longitudinal momentum and the angle with respect to the incident projectile direction, respectively. This can be compared to the definition of rapidity y, which is additive under Lorentz boosts ($c=1$),

$$y=\tfrac{1}{2}\ln\left[\frac{E+p_z}{E-p_z}\right]\ , \tag{2}$$

where E is the total energy of the particle. For massless particles $\eta=y$. For pions the difference between η and y is generally insignificant since their mean transverse momentum is large compared to their mass $m_\pi=139$ MeV, i.e., typically $\langle p_T\rangle\approx 350$ MeV/c, so that $\eta-y\approx\ln(m_T/p_T)=0.07$, where $m_T^2=p_T^2+m_\pi^2$. For kaons the difference is greater, and for protons the difference is greater still. Since most of the charged secondaries at these energies are pions, the distinction between η and y on the whole is not too significant. Anyway, since here one does not have momentum measurements in emulsions, η is what we must use.

In Fig. 1 we show the pseudorapidity distribution at 14.6A GeV, averaged over 107 events, and in Fig. 2 we show the pseudorapidity distribution averaged over the 31 highest multiplicity events ($N_s\geq 208$) at 200A GeV. It can be seen immediately that the distributions do not exhibit a midrapidity plateau. Bjorken's model assumes this and also complete transparency of the nuclei. Thus, even for the highest multiplicity events at 200A GeV, Bjorken's scaling-hydrodynamic model[9] cannot be applied. If that model has some applicability, then presumably one must go to much higher energies, perhaps the 100+100A GeV heavy-ion collider RHIC. The JACEE collaboration has in fact reported one event of Ca+C at 100A TeV where a flat pseudorapidity plateau is observed over six units of pseudorapidity.[10]

Another extreme model we may consider is a single fireball formed at midrapidity which subsequently explodes, spraying out particles isotropically in its own rest

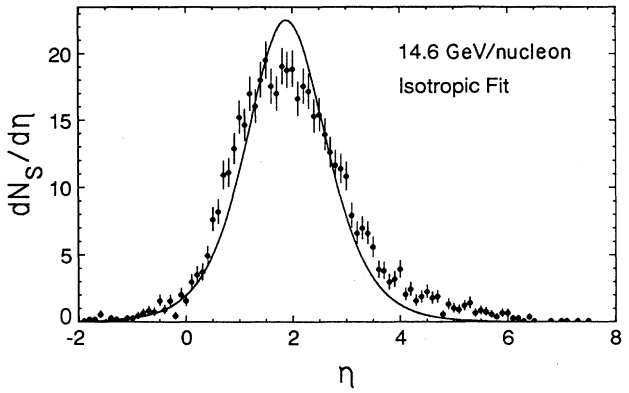

FIG. 1. N_s pseudorapidity distribution in ^{16}O+AgBr collisions at 14.6A GeV averaged over the number of events. The solid line is the best fit using Eq. (5), with normalized $\chi^2=6.35$ for the range $0.0\leq\eta\leq 5.0$. Only statistical errors are shown.

frame. In that frame the angular distribution is

$$\frac{dN_s}{d\Omega_F}=\frac{N_s}{4\pi}\ , \tag{3}$$

which becomes, in terms of pseudorapidity,

$$\frac{dN_s}{d\eta_F}=\frac{N_s}{2}\frac{1}{(\cosh\eta_F)^2}\ . \tag{4}$$

In the laboratory frame (assuming massless pions)

$$\frac{dN_s}{d\eta}=\frac{N_s}{2}\frac{1}{[\cosh(\eta-y_F)]^2}\ , \tag{5}$$

where $y_F=\tanh^{-1}v_F$ is the fireball rapidity and v_F its velocity in the laboratory frame. A good approximation to an isotropic distribution is a Gaussian with a width $\delta\approx 0.88$,

$$\frac{dN_s}{d\eta_F}\approx\frac{N_s}{(2\pi\delta^2)^{1/2}}\exp\left[-\frac{\eta_F^2}{2\delta^2}\right]\ , \tag{6}$$

which has been used in several cluster models and gives a

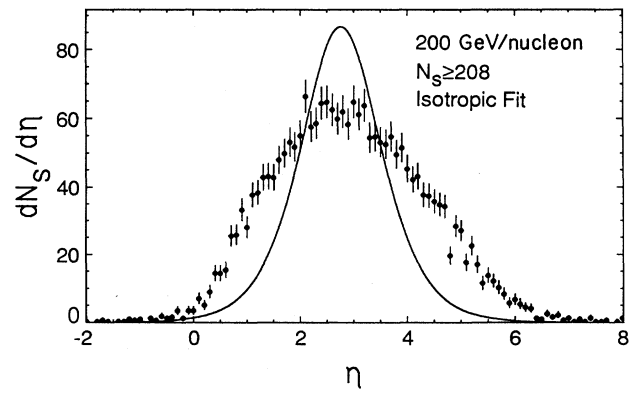

FIG. 2. N_s pseudorapidity distribution in ^{16}O+AgBr at 200A GeV averaged over 31 events with $N_s\geq 208$. The solid line is the best fit using Eq. (5), with normalized $\chi^2=28.2$ for the range $0.0\leq\eta\leq 6.0$. Only statistical errors are shown.

cluster size of roughly one pseudorapidity unit. The functional form (5) was fit to the data, and the best results are shown in Figs. 1 and 2. The idea of isotropic decay of a single fireball is roughly consistent with the 14.6 A-GeV data, but is definitely ruled out by the 200 A-GeV large multiplicity data set (see the figure captions for the respective χ^2's).

We have made a best fit to the data assuming a Gaussian distribution

$$\frac{dN_s}{d\eta} = \frac{N_s}{(2\pi\sigma^2)^{1/2}} \exp\left[-\frac{(\eta-\eta_0)^2}{2\sigma^2} \right] . \quad (7)$$

The fits are shown in Figs. 3–5 for the 14.6 A, 60 A, and 200 A-GeV data, which was averaged over 107, 226, and 146 events, respectively. Figure 6 shows the fit to the 200 A-GeV data ($N_s \geq 208$), which was averaged over 31 events. In each case a Gaussian seems to be an economical way to parametrize the data. (We have also fitted these data using two shifted isotropic distributions, obtaining much better χ^2's then with a single isotropic distribution, but still never as good as those obtained using Gaussians.)

The fit parameters are shown in the Table I. A number of points can be made. The distributions are approximately centered at the nucleon-nucleon center-of-mass (c.m.) rapidity. The difference between η_0 and $y^{NN}_{\text{c.m.}}$ (the nucleon-nucleon center-of-mass rapidity) might be due to the difference between rapidity and pseudorapidity and to the asymmetry between target and projectile; the former tends to make $\eta_0 > y^{NN}_{\text{c.m.}}$, whereas the later tends to make $\eta_0 < y^{NN}_{\text{c.m.}}$. The trigger $N_h > 15$, together with the condition that there are no fragments with $Z \geq 2$ and the $N_s \geq 208$, means that there is complete overlap of the oxygen with the target nucleus, so that the effective target-projectile asymmetry in baryon number is probably more like 2 or 3 to 1 (when one ignores spectator nucleons) rather then 5 or 7 to 1. Small deviations from the Gaussian fits at the tails of the distributions may be a consequence of the two aforementioned reasons plus some small proton contamination. The width increases monotonically with beam energy, but from the two 200 A-GeV data sets we have studied does not seem to depend on the multiplicity, at least for the trigger we have chosen.[11]

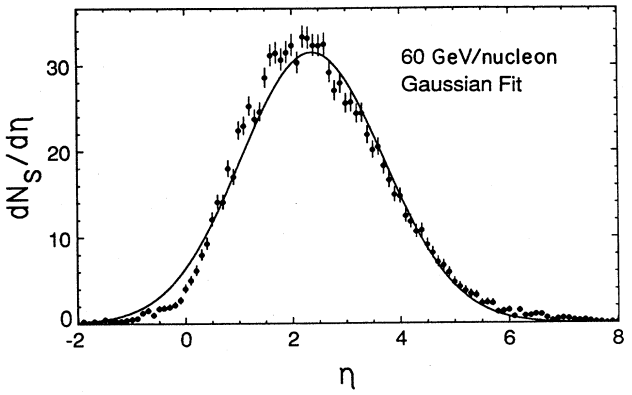

FIG. 4. N_s pseudorapidity distribution in ^{16}O+AgBr at 60 A GeV averaged over all events. The solid line is the best fit using a Gaussian, Eq. (7), with normalized $\chi^2 = 4.30$ for the range $0.0 \leq \eta \leq 6.0$. Only statistical errors are shown.

It is interesting to compare these results to pp collisions at the same energy. Carruthers and Duong-Van[12] present the pseudorapidity distributions for pp collisions at 205 GeV and fit them to a Gaussian in *rapidity* taking into account the exponential p_T distribution of the secondaries. Very good fits are obtained for $\sigma = 1.53$, which is just what the Landau model predicts for 205 GeV. Klar and Hüfner[13] analyze rapidity distributions for pp, pAr, and pXe collisions from a streamer-chamber experiment at 200 GeV,[14] which, due to the presence of a magnetic field, can separate positive from negative particles and measure their momentum, thus obtaining the rapidity, as opposed to the pseudorapidity, of the secondaries. A fit using two identical but shifted Gaussians reproduces well the *negative* particle rapidity distribution. Since kaons

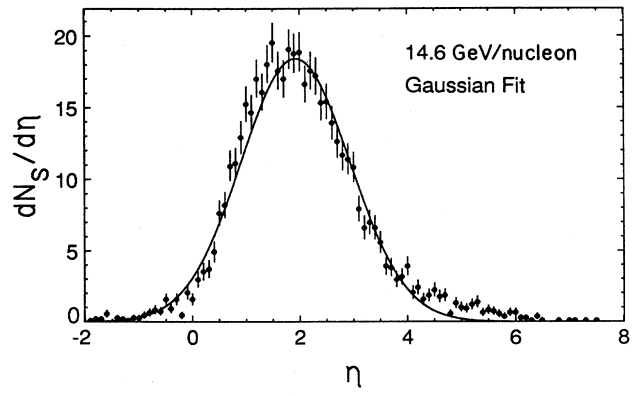

FIG. 3. N_s pseudorapidity distribution in ^{16}O+AgBr at 14.6 A GeV averaged over all events. The solid line is the best fit using a Gaussian, Eq. (7), with normalized $\chi^2 = 2.8$ for the range $0.0 \leq \eta \leq 5.0$. Only statistical errors are shown.

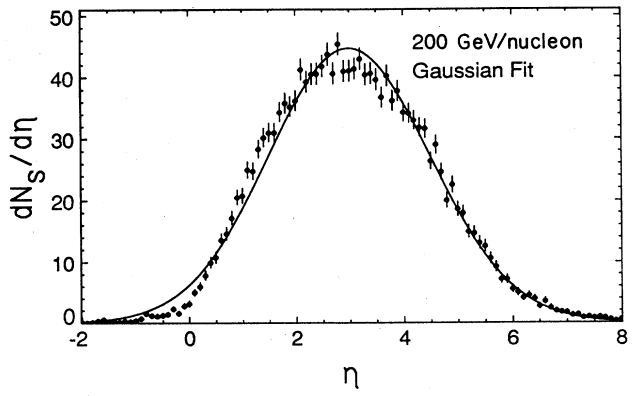

FIG. 5. N_s pseudorapidity distribution in ^{16}O+AgBr at 200 A GeV averaged over all events. The solid line is the best fit using a Gaussian, Eq. (7), with normalized $\chi^2 = 3.51$ for the range $0.0 \leq \eta \leq 6.0$. Only statistical errors are shown.

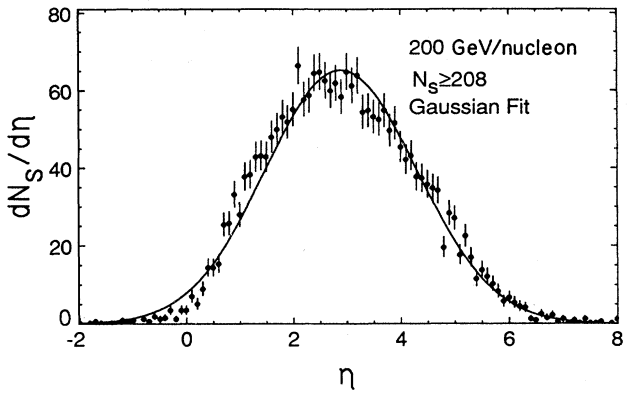

FIG. 6. N_s pseudorapidity distribution in $^{16}O+AgBr$ at 200A GeV averaged over 31 events with $N_s \geq 208$. The solid line is the best fit using a Gaussian, Eq. (7), with normalized $\chi^2=2.14$ for the range $0.0 \leq \eta \leq 6.0$. Only statistical errors are shown.

and antiprotons are less then 10% and 1% of the produced particles, respectively, this distribution is composed mainly of pions and is furthermore symmetric about $y^{NN}_{\text{c.m.}}$. We have fitted these data quite well using a single Gaussian with a width $\sigma=1.53$, with small deviations at the tails. It therefore seems that at 200-GeV pp pseudorapidity and rapidity distributions can be well accounted for by the Landau model.

We have, therefore, analyzed the nucleus-nucleus pseudorapidity distributions previously mentioned in terms of Landau's hydrodynamical model.[15] Assuming an equation of state of the form $P=c_0^2\varepsilon$, where P is the pressure, ε the energy density, and c_0 is the (constant) speed of sound, Landau's model predicts a rapidity distribution which is, to good approximation, a Gaussian. The width is given by[16]

$$\sigma_L^2=\tfrac{8}{3}\frac{c_0^2}{1-c_0^4}\ln\gamma_{\text{c.m.}} . \tag{8}$$

Here $\gamma_{\text{c.m.}}$ is the Lorentz contraction factor in the projectile-target center-of-mass frame, assuming $A+A$ collisions (the effects of spectator nucleons are completely ignored). Taking $c_0^2=\frac{1}{3}$, a not unnatural choice for a high-temperature gas and $\gamma_{\text{c.m.}}$ in the nucleon-nucleon center-of-mass frame, we obtain the widths shown in Table I. The values of σ_L agree with the measured widths in all four cases within the error bars. This agreement could be accidental (e.g., a result of phase space limits). Nevertheless one should examine the consequences of this model.

Landau's originally published concept was that the incident projectile and target (protons then) would stop each other in one Lorentz contracted (proton) volume in the c.m. frame. This Lorentz contracted pancake then would expand hydrodynamically, primarily along the beam axis. When the temperature or energy density was low enough the produced particles, mostly pions, would lose thermal contact and would free stream towards the detectors.

This scenario is unnecessarily restrictive for our purposes. In order to obtain a Gaussian rapidity distribution all that is required is that (1) particle production and thermalization occurs in an ellipsoid oriented along the beam axis with the ratio of semi-major to semi-minor axes given by $\gamma_{\text{c.m.}}$, (2) the produced matter undergoes a hydrodynamic expansion with the equation of state $P=c_0^2\varepsilon$, and (3) the expanding matter maintains thermal contact down to low-energy density, low enough so that $\varepsilon_{\text{initial}}/\varepsilon_{\text{final}} \gg 1$. The width is then given by Eq. (8). Note that it is not necessary to assume complete stopping of the projectile. This scenario is similar to that envisioned by the Pokorski–Van Hove model,[17,18] where the incident valence quarks are considered approximately transparent to each other, but not the gluons which interact more strongly, producing a "confined gluon cloud" (thermalized?) in the central region.[19,20] The general view of strong interactions as "soft"[21] (i.e., jets are a very small percentage of the total pp cross section), which has emerged from experiments in hadron physics in the last two decades, lends further support to this scenario.

During a nonviscous hydrodynamic expansion the total entropy S is conserved. If the particle masses are smaller than the temperature at the time thermal contact is broken, such as for pions, the relationship between entropy and particle number is $S \approx 3.7N$. So, to know the entropy produced initially we only need to know the number of produced particles. The initial volume may be estimated, following Landau's assumptions, as the volume of an oxygen nucleus Lorentz contracted by a factor of $\gamma_{\text{c.m.}}$. The estimate of the initial entropy density s_{initial} is, therefore,

TABLE I. The best-fit Gaussian parameters from the KLM data and Landau's model prediction for the widths.

	14.6A GeV all N_s	60A GeV all N_s	200A GeV all N_s	200A GeV $N_s \geq 208$
N_s	$5 \leq N_s \leq 78$	$24 \leq N_s \leq 171$	$30 \leq N_s \leq 290$	$208 \leq N_s \leq 290$
σ	1.02±0.03	1.33±0.02	1.51±0.02	1.41±0.15
η_0	1.92±0.03	2.37±0.02	2.99±0.02	2.89±0.15
$y^{NN}_{\text{c.m.}}$	1.75	2.43	3.03	3.03
σ_L	1.03	1.31	1.53	1.53

TABLE II. The entropy density according to Landau's model.

	14.6A GeV all N_s	60A GeV all N_s	200A GeV all N_s	200A GeV $N_s \geq 208$
$\langle N_s \rangle$	49.6±1.3	106.2±2.3	169±3.9	233
$\langle s_{\text{initial}} \rangle$	4.6 fm^{-3}	24 fm^{-3}	75 fm^{-3}	105 fm^{-3}

$$s_{\text{initial}} = \tfrac{3}{4}\gamma_{\text{c.m.}} \frac{(N_s - A_p)}{A_p} \text{ fm}^{-3} . \tag{9}$$

Here we take the projectile radius as $1.2A_p^{1/3}$ fm, subtract twice the number of projectile protons from the number of charged secondaries as an estimate of the number of relativistic wounded protons from the projectile and target and multiply by $\frac{3}{2}$ to estimate the number of produced particles. In Table II we give the average initial entropy density for the different energies and multiplicity cuts. The entropy formula given in (9) may be as much as a factor of 2 too high, due to the expected diffuseness of the surface of the initial volume of the produced matter. Even so, there is a noticeable difference in s_{initial} as we go from 14.6A and 60A GeV to 200A GeV. These entropy estimates could be compared to the entropy of a bag model equation of state which exhibits a first-order phase transition[22,23] between a gas of pions and a quark-gluon gas. Taking the critical temperature $T_c = 200$ MeV, one finds that

$$\begin{aligned} s_\pi &= 1.3 \left[\frac{T}{T_c}\right]^3 \text{fm}^{-3} , \\ s_{qg} &= 16 \left[\frac{T}{T_c}\right]^3 \text{fm}^{-3} . \end{aligned} \tag{10}$$

This may suggest that the 14.6- and 60-GeV collisions produce matter roughly in the mixed phase (presently, there is probably an uncertainty of ±50 MeV in T_c), while the 200-GeV collision produces matter in the quark-gluon plasma phase.

Though the agreement between the pseudorapidity distributions in Landau's model and data is interesting, it is perhaps premature to accept the model's validity solely on this basis. There are theoretical and experimental reasons to doubt its validity,[19,24] at least for higher energies, since a plateau is expected to develop in the intermediate rapidity region and an inside-outside cascade picture will probably be more appropriate to describe the dynamical evolution of the system.[9,25] In particular, Landau's assumption of arbitrarily thin Lorentz contracted nuclei probably breaks down above 200 GeV, since the nuclear thickness should then saturate to about 1 fm due to the wee parton distribution (i.e., low-momentum partons are always present in the proton). Evidence for partial transparency has, in fact, been reported for 200A GeV collisions.[25] But, from 10A–200A GeV, Landau's model (or variations thereof[26,27]) seems to be more appropriate to simulate nucleus-nucleus collisions. We also note that detailed comparisons with dynamical simulation models, such as those of Lund Fritiof[28] and Venus,[29] need to be done.

III. TWO-PARTICLE AZIMUTHAL CORRELATIONS

Following Basile *et al.*[30] (see also Ref. 31 and the discussion in Ref. 32, p. 21) we studied azimuthal correlations among the secondaries in the following way. First pick a reference particle with pseudorapidity η_1 and azimuth ϕ_1. Now we look a distance $\Delta\eta$ away from η_1, at a bin centered at $\eta_2 = \eta_1 + \Delta\eta$ with width $\delta\eta$. Within that bin we count the number of secondaries $N_<$ which emerge on the same side as the reference particle, and we count the number of secondaries $N_>$ which emerge on the opposite side of the reference particle. In other words, if ϕ_i is the azimuthal angle of the ith particle in the bin, then it counts towards $N_<$ if $|\phi_i - \phi_1| < \pi/2$, and it counts towards $N_>$ if $|\phi_i - \phi_1| > \pi/2$. (Here we take $-\pi < \phi_1 - \phi_i \leq \pi$.) The azimuthal correlation function is defined as

$$B(\eta_1, \Delta\eta) = \frac{N_> - N_<}{N_> + N_<} . \tag{11}$$

Obviously $-1 \leq B \leq 1$. If all the particles in the bin are emitted on the same side as the reference particle then $B = -1$, and if they are emitted on the opposite side then $B = 1$. An absence of correlation would yield $B = 0$.

There are several reasons to expect $B \neq 0$. Transverse momentum conservation would suggest $B > 0$. Formation of clusters (resonances or minifireballs) with $p_T \neq 0$ would suggest $B < 0$ for $\Delta\eta \leq \delta = 0.88$. Bounce off of the projectile from the target would suggest $B > 0$ for large values of $\Delta\eta$, but $B < 0$ for small values of $\Delta\eta$.

In pp collisions at these energies one finds[30] typically that $B(\eta_1, \Delta\eta = 0) = 0.10$. B falls monotonically with increasing $|\Delta\eta|$ until it reaches a value of about 0.05 at $|\Delta\eta| = 0.6$, and remains at 0.05 for $|\Delta\eta| > 0.6$.

Here we concentrate on the 200A-GeV data and, in order to maximize statistics, we concentrate on 123 events with $N_s > 120$ out of the 146 events of our ^{16}O+AgBr data set; the lower-energy data gives similar results. In Figs. 7(a)–7(c) we plot B vs $\Delta\eta$ for $\eta_1 = 3$, 4, and 5, respectively. In all three cases it may be seen that $|B| < 0.10$ for all values of $\Delta\eta$. In fact, with the statistics available, B is consistent with zero. No pattern of azimuthal asymmetry is evident.

To infer a signal for B would require the error bars to be at least a factor of 3 smaller, which means analyzing ten times as many events. Since B is essentially a two-particle correlation function it would be better to measure it using high-statistics electronic detectors instead of emulsions.

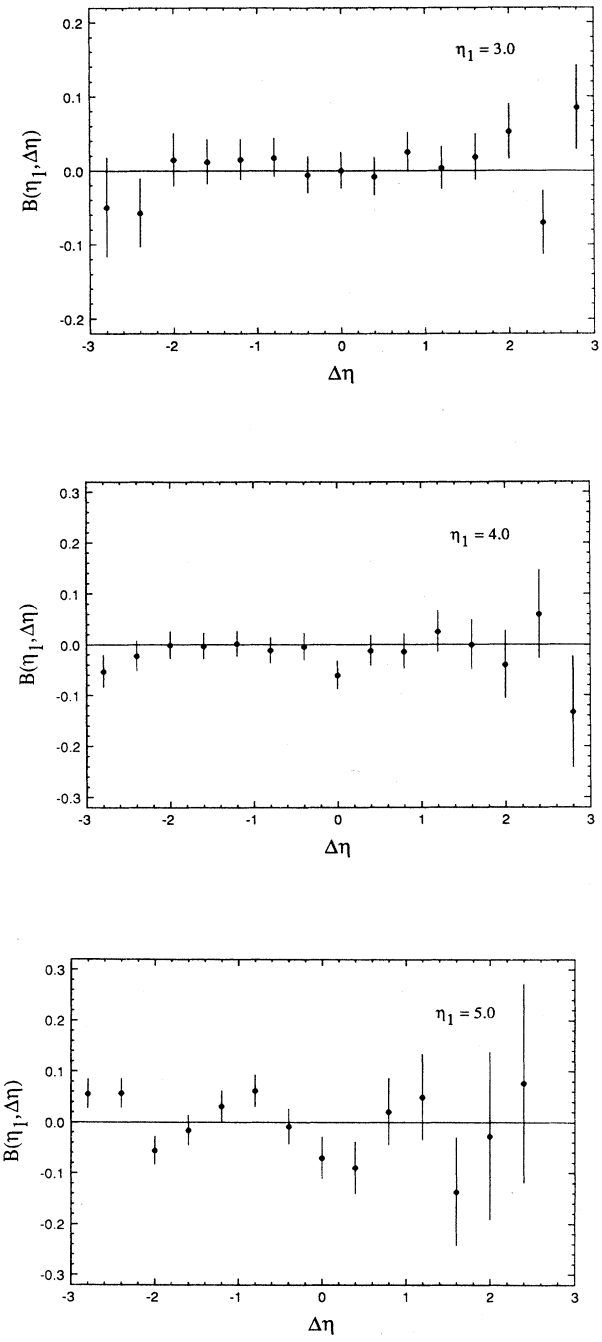

FIG. 7. (a) The azimuthal asymmetry correlation function $B(\eta_1,\Delta\eta)$, for 123 events with $N_s \geq 120$ and with a pseudorapidity bin size $\delta\eta=0.4$, at 200A GeV. The value of η_1 is the first particle in the interval (2.98,3.02). (b) The azimuthal asymmetry correlation function $B(\eta_1,\Delta\eta)$, for 123 events with $N_s \geq 120$ and with a pseudorapidity bin size $\delta\eta=0.4$, at 200A GeV. The value of η_1 is the first particle in the interval (3.98,4.02). (c) The azimuthal asymmetry correlation function $B(\eta_1,\Delta\eta)$, for 123 events with $N_s \geq 120$ and with a pseudorapidity bin size $\delta\eta=0.4$, at 200A GeV. The value of η_1 is the first particle in the interval (4.98,5.02).

IV. TWO-PARTICLE PSEUDORAPIDITY CORRELATION

The normalized two-particle pseudorapidity correlation function $R(\eta_1,\eta_2)$ is defined as[33,34]

$$R(\eta_1,\eta_2)=\frac{d^2N_s/d\eta_1 d\eta_2}{(dN_s/d\eta_1)(dN_s/d\eta_2)}-1 . \tag{12}$$

Operationally one divides the pseudorapidity axis into bins of width $\Delta\eta$. Then, for a given event

$$\frac{dN_s^{\text{event}}}{d\eta}=\frac{n}{\Delta\eta} \tag{13}$$

and

$$\frac{d^2N_s^{\text{event}}}{d\eta_1 d\eta_2}=\begin{cases}\dfrac{n_1 n_2}{(\Delta\eta)^2} & \text{for } \eta_1\neq\eta_2 , \\ \dfrac{n_1(n_2-1)}{(\Delta\eta)^2} & \text{for } \eta_1=\eta_2 ,\end{cases} \tag{14}$$

where n, n_1, and n_2 are the number of secondaries in the bins centered at η, η_1, and η_2 in that event and N_s^{event} is the multiplicity of that event. Averaging over events

$$\frac{dN_s}{d\eta}=\frac{1}{N_{\text{events}}}\sum_{\text{events}}\frac{dN_s^{\text{event}}}{d\eta} , \tag{15}$$

$$\frac{d^2N_s}{d\eta_1 d\eta_2}=\frac{1}{N_{\text{events}}}\sum_{\text{events}}\frac{d^2N_s^{\text{event}}}{d\eta_1 d\eta_2} . \tag{16}$$

$R(\eta_1,\eta_2)$ is plotted in Fig. 8 for all three energies with the first particle fixed at midrapidity, $\eta_1=y_{\text{c.m.}}^{NN}$. A positive correlation is observed for the full range of $\eta_1-\eta_2$.

Mixing of events with different multiplicities can lead to artificial correlations. To remove the effect we follow the method suggested in Ref. 35. We calculate the pseudocorrelation function as

$$R^{\text{pseudo}}(\eta_1,\eta_2)=\frac{1}{D^2}(N_1-N_s)(N_2-N_s)-\frac{1}{N_s} , \tag{17}$$

where N_s is the mean multiplicity and D^2 is the dispersion in multiplicity

$$D^2=\frac{1}{N_{\text{events}}}\sum_{\text{events}}(N_s^{\text{event}})^2-N_s^2 \tag{18}$$

and

$$N_i=\frac{\sum_{\text{events}} n_i N_s^{\text{event}}}{\sum_{\text{events}} n_i} \quad \text{with } i=1,2 . \tag{19}$$

Then the corrected correlation function is computed from

$$R^{\text{corrected}}(\eta_1,\eta_2)=R(\eta_1,\eta_2)-R^{\text{pseudo}}(\eta_1,\eta_2) . \tag{20}$$

Error bars were computed using the formulas in the appendix of Ref. 35.

The multiplicity-corrected correlation function is plotted in Fig. 9 for all three beam energies. Within the error

bars there is no evidence for two-particle correlations. The results are consistent with independent emission of the secondaries.[36] However, any correlations which are present in *pp* collisions, such as those due to the decay of resonances such as ρ, are likely to be diluted by the high multiplicities in nucleus-nucleus collisions. Unfortunately, it seems also that the correlation functions we used here are not sensitive enough to observe intermittency correlations,[37,38] which have been observed by us by calculating factorial moments in Ref. 39.

V. PSEUDORAPIDITY GAP DISTRIBUTIONS

Since an emulsion is a 4π detector which is able to measure the angles of all charged particles one should be able to extract more information than just one (Sec. II) and two (Secs. III and IV) particle distributions. A more global picture of the events is provided by the n-gap distribution functions.[40,41] These distributions are defined in the following way. On an event by event basis, order the secondaries according to pseudorapidity. The zero-gap r is defined to be the difference in pseudorapidity between adjacent particles, $\eta_{i+1}-\eta_i$. The n-gap r is defined to be the difference in pseudorapidity between particles which are separated by n particles, $\eta_{i+n+1}-\eta_i$. The n-gap distribution function $P_n(r)$ is the distribution of the n-gap r, averaged over some class of events.

Before analyzing the data let us consider what would be expected if the secondaries were distributed randomly along the pseudorapidity axis with average density

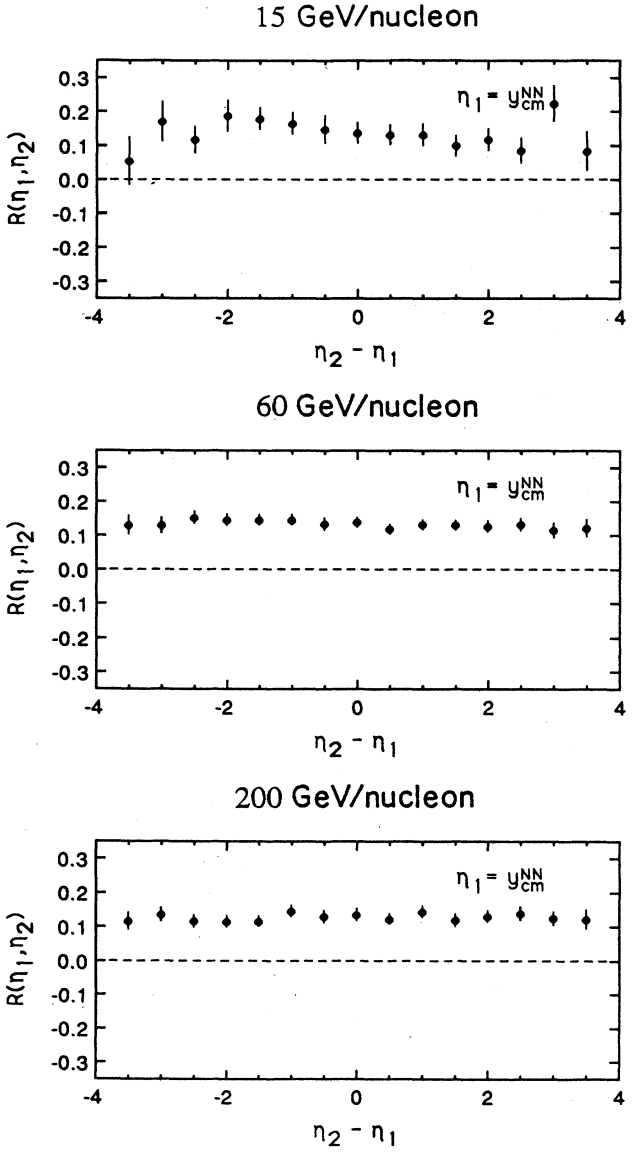

FIG. 8. The multiplicity uncorrected two-particle pseudorapidity correlation function $R(\eta_1,\eta_2)$ [Eq. (12)] at 14.6A, 60A, and 200A GeV.

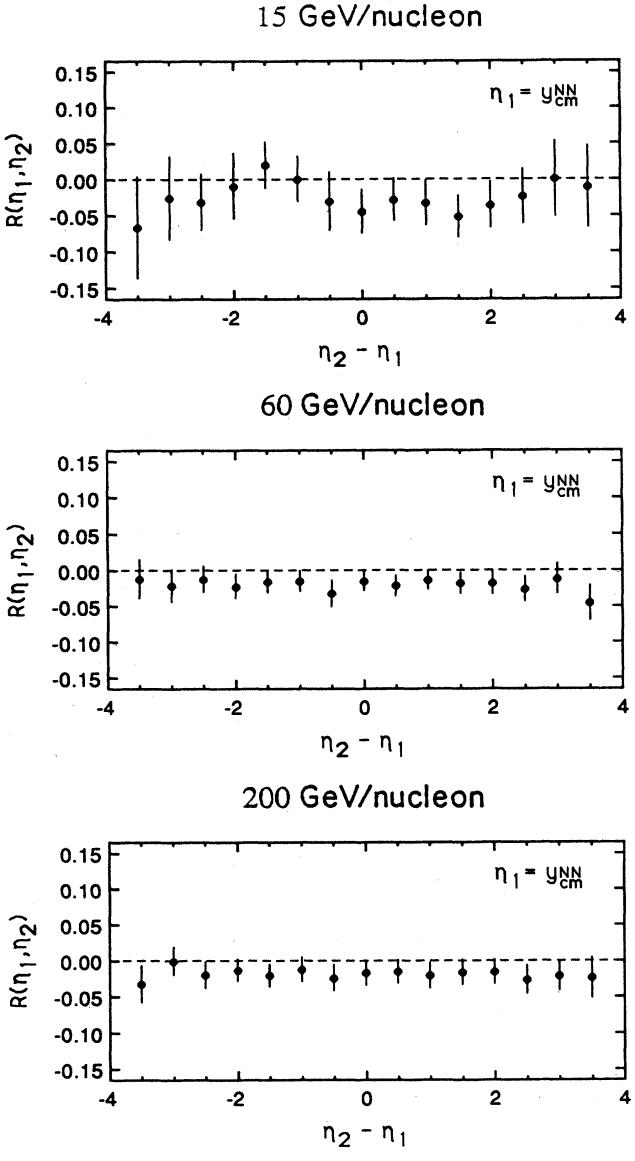

FIG. 9. The multiplicity corrected two-particle pseudorapidity correlation function $R^{\text{corrected}}(\eta_1,\eta_2)$ [Eq. (20)] at 14.6A, 60A, and 200A GeV.

$dN_s/d\eta=\rho_s=$constant (flat pseudorapidity distribution). Then the probability to find two particles separated by a distance r and containing exactly n particles within the gap is a Poisson distribution

$$P_n(r)=\frac{(\rho_s r)^n}{n!}\exp(-\rho_s r) . \tag{21}$$

In particular, $P_0(r)=\exp(-\rho_s r)$.

Now let us assume that the secondaries are not emitted independently, but first clusters are formed, and these clusters decay isotropically into the observed secondaries. Physically, these clusters may be ordinary hadronic resonances such as ρ and ω or, in nucleus-nucleus collisions, they may be droplets of quark-gluon plasma surrounded by hadronic gas.[42] The latter may be a manifestation of passage through a phase mixture if there is a first-order deconfinement phase transition. Following the work of Quigg, Pirila, and Thomas[40] we know that in such a cluster model the behavior of the 0-gap distribution is

$$P_0(r)\sim\begin{cases}\exp(-\rho_s r) & \text{for small } r ,\\ \exp(-\rho_c r) & \text{for large } r .\end{cases} \tag{22}$$

When r is less than the width of a cluster in pseudorapidity, $r<\delta\approx 0.9$, one expects the secondaries to be emitted independently. Hence the exponential decay. When r is larger than the width of a cluster, $r>\delta\approx 0.9$, one expects the two observed particles to be emitted from different clusters. Hence $P_0(r)$ will then measure the cluster rapidity density ρ_c. Note that $\rho_s=\langle m\rangle\rho_c$, where $\langle m\rangle$ is the mean number of decay products of a cluster and ρ_c is the mean cluster density. In fact experimental results are often parametrized as

$$P_0(r)=A\exp(-\rho_s r)+B\exp(-\rho_c r) . \tag{23}$$

This yields a curve which is concave upward on a semilogarithmic graph,[40,41,43] but note that these results assume flat distributions in pseudorapidity.

In Fig. 10 we plot $P_0(r)$ for the 31 highest multiplicity events, $N_s>208$, at $200A$ GeV. We restrict ourselves first to the central two units of pseudorapidity, $2<\eta<4$, since we anticipate this is where the most interesting physics will be. The data fall off exponentially with r with a slope of about $\rho_s=57$. This is the observed mean pseudorapidity density in this interval (cf. Figs. 2 or 6). Unfortunately, due to the large value of ρ_s ($\rho_s\approx 2$ in pp collisions at this energy[12,44]) the gap distribution falls off so rapidly that we run out of data at $r\approx 0.1$ to 0.15. Since this is less than the width of a cluster we have no hope of measuring ρ_c, or the mean cluster size, in this way.

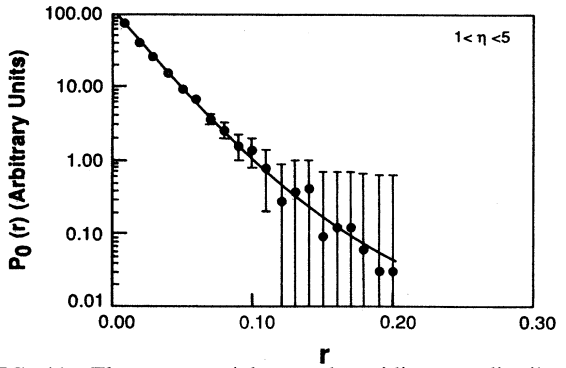

FIG. 11. The zero-particle pseudorapidity gap distribution $P_0(r)$ for particles within the interval $1<\eta<5$. The solid curve is the result of a Monte Carlo simulation assuming independent-particle emission.

In Fig. 11 we again plot $P_0(r)$ but this time for the extended pseudorapidity window $1<\eta<5$, in hopes of increasing the dynamic range of r. After falling three decades we run out of data at $r\approx 0.15$ to 0.20. There is a curvature to the spectrum so one may be tempted to apply Eq. (23) to determine ρ_c. This would be *wrong* due to the fact that $\rho_s=dN_s/d\eta$ is not flat. Also, since the uncertainty in measuring η in the range $1<\eta<5$ is typically in the range 0.02 to 0.08, the $P_0(r)$ distribution is statistically not significant for these large density events, unlike pp collisions where $P_0(r)$ extends to $r\approx 2.5$.[40] Nevertheless, we include these distributions here to emphasize the fact that the curvature in $P_0(r)$ for $1<\eta<5$ is not an immediate indication of clustering, but rather just reflects the Gaussian structure of the pseudorapidity distributions. Since many previous papers have claimed this curvature is an indication of cluster formation we consider

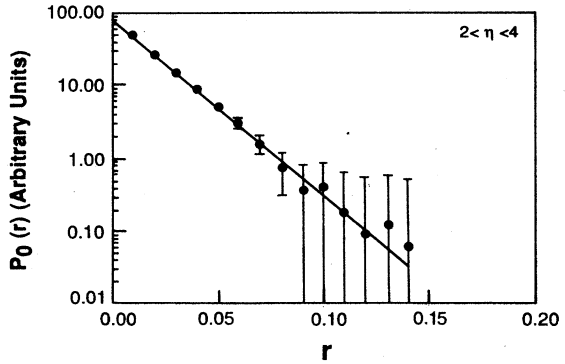

FIG. 10. The zero-particle pseudorapidity gap distribution $P_0(r)$ for particles within the interval $2<\eta<4$. The solid curve is the result of a Monte Carlo simulation assuming independent-particle emission.

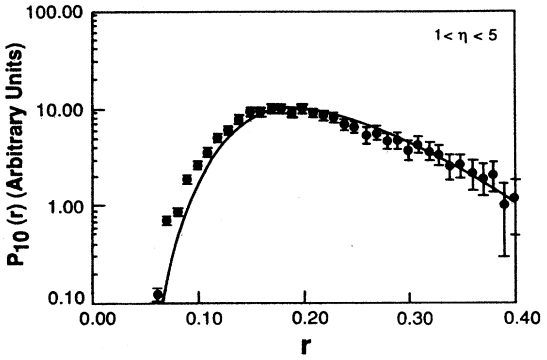

FIG. 12. The ten-particle pseudorapidity gap distribution $P_{10}(r)$ for particles within the interval $1<\eta<5$. The solid curve is the result of a Monte Carlo simulation assuming independent-particle emission.

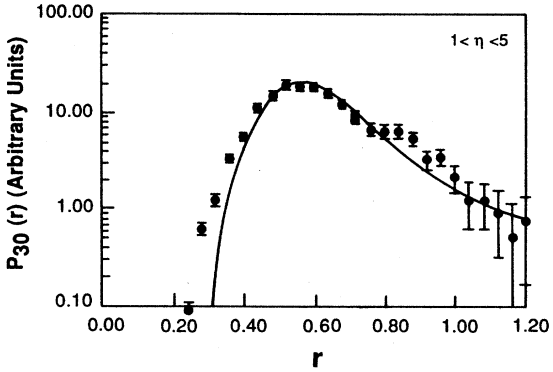

FIG. 13. The 30-particle pseudorapidity gap distribution $P_{30}(r)$ for particles within the interval $1<\eta<5$. The solid curve is the result of a Monte Carlo simulation assuming independent-particle emission.

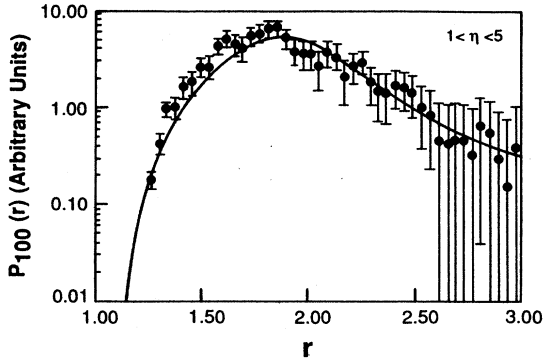

FIG. 15. The 100-particle pseudorapidity gap distribution $P_{100}(r)$ for particles within the interval $1<\eta<5$. The solid curve is the result of a Monte Carlo simulation assuming independent-particle emission.

this an important point to clear up in the literature.

To handle the Gaussian nature of the single-particle pseudorapidity distribution we have written a Monte Carlo event generator. This computer code generated events which matched the multiplicity distribution of the data. It assigned pseudorapidities to the particles according to a Gaussian pseudorapidity distribution with the same width as the data. For this the Box-Muller method for generating random Gaussian deviates was used.[45] This set of events, which have no correlations among the particles, was then used in the same computer program which obtained the gap distributions from the data. The results are shown as the solid curves in Figs. 10 and 11. No evidence is seen for deviations from independent-particle emission.

In Figs. 12–15 we plot $P_{10}(r)$, $P_{30}(r)$, $P_{50}(r)$, and $P_{100}(r)$. By making n larger we can study larger values of the gap r.[46] The peak of the distribution $P_n(r)$, for $n>0$, shifts to larger values of r as n increases. This is expected on the basis of the Poisson distribution discussed earlier. Beyond the peak the data fall less rapidly than a Poisson, a consequence of the Gaussian nature of the pseudorapidity distribution. The independent-particle generator describes the data reasonably well, although one may notice occasional deviations. These deviations occur to the left of the peak for $n=10$, 20, and 30. There are also hints of structure to the right of the peak for $n=30$, 50, and 100. More sophisticated event generators are probably needed to determine the significance of these deviations.

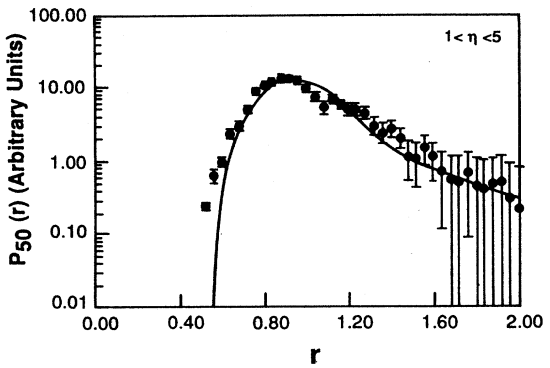

FIG. 14. The 50-particle pseudorapidity gap distribution $P_{50}(r)$ for particles within the interval $1<\eta<5$. The solid curve is the result of a Monte Carlo simulation assuming independent-particle emission.

VI. CONCLUSION

We have established that the single-particle pseudorapidity distribution is Gaussian in shape at $14.6A$, $60A$, and $200A$ GeV to a very good approximation, over the full range of pseudorapidity, from target to projectile, though small deviations are seen at low pseudorapidities. The width of the Gaussians are fairly independent of multiplicity when the impact parameter is small enough for complete overlap of projectile and target and increase logarithmically with the center-of-mass energy, whereas the growth in height is dependent on the multiplicity N_s, the center-of-mass energy, and the impact parameter. All these features are in agreement with Landau's model. Although the measurements of E_T distributions by other experiments seem to indicate a large degree of stopping of the incident nucleus,[47,48] we emphasize that the agreement of Landau's model with our experimental pseudorapidity distributions does not necessarily imply large stopping (as noted by Gyulassy[49] none of the present experiments can distinguish high rapidity protons). From Landau's model we inferred an initial entropy which is great enough to make quark-gluon plasma at $200A$ GeV. A mixed phase is probably formed at $14.6A$ and $60A$ GeV. These results negate the applicability of Bjorken's scaling hydrodynamical model at these energies. An isotropic fireball model is also ruled out by the data.

We next examined two-particle azimuthal and pseudorapidity distributions, where no evidence for correlations was found. These correlations are probably masked by the high multiplicity of these events. To obtain a more global view of these nucleus-nucleus collisions, including possible many-body long-range correlations and search for cluster formation, we then examined n-gap dis-

tributions in 31 high-multiplicity events at 200A GeV, where there are $n=0$, 10, 30, 50, and 100 particles in the pseudorapidity gap (note that only emulsions and streamer chambers have measurements exclusive enough to observe n-gap distributions). Taking the uncertainty in measurements of pseudorapidity into account, this allows us to study gaps from 0.1 to 3.0 units of pseudorapidity. The results are consistent with the independent emission of secondaries. No evidence for the formation of large clusters was found. In a future paper we plan to include studies of n-gap distributions at 14.6A and 60A GeV and to include results from the sulfur beam.

ACKNOWLEDGMENTS

H. v. G. would like to thank E. L. Feinberg, M. Gyulassy, A. Krzywicki, and T. Matsui for very instructive conversations. He is also much obliged to J.-P. Blaizot, A. Morel, and M. Soyeur for discussions and hospitality at CEN Saclay, Gif-sur-Yvette, France. This work was supported in part by the U.S. Department of Energy Grant No. DE-FG02-87ER40328 and by the National Science Foundation Grants Nos. PHY-8604315 Louisiana State University (LSU) and PHY-8611864 University of Minnesota (UM).

[1]For a recent general review, see Proceedings of the Sixth International Conference on Ultra-Relativistic Nucleus-Nucleus Collisions—Quark Matter, Nordkirchen 1987 [Z. Phys. C **38**, A3 (1988)].

[2]L. M. Barbier *et al.*, KLM Collaboration, Phys. Rev. Lett. **60**, 405 (1988).

[3]J. Schukraft, Z. Phys. C **38**, 59 (1988).

[4]I. Otterlund, Z. Phys. C **38**, 65 (1988).

[5]F. Corriveau *et al.*, Helios Collaboration, Z. Phys. C **38**, 15 (1988).

[6]W. Heck *et al.*, NA35 Collaboration, Z. Phys. C **38**, 19 (1988).

[7]H. R. Schmidt *et al.*, WA80 Collaboration, Z. Phys. C **38**, 109 (1988); R. Albrecht, *et al.*, Phys. Lett. B **199**, 297 (1988).

[8]T. W. Atwater, P. S. Freier, and J. I. Kapusta, Phys. Lett. B **199**, 30 (1987).

[9]J. D. Bjorken, Phys. Rev. D **27**, 140 (1983).

[10]T. H. Burnett *et al.*, JACEE Collaboration, Phys. Rev. Lett. **50**, 2062 (1983).

[11]For silicon (^{28}Si) at 14.6 (154 events with $\langle N_s \rangle = 92.3 \pm 2.3$) and sulfur (^{32}S) at 200A GeV (45 events with $\langle N_s \rangle = 286.7 \pm 9.7$), the distributions are also Gaussian with widths of 1.07 ± 0.06 and 1.59 ± 0.05, respectively.

[12]P. Carruthers and Minh Duong-Van, Phys. Rev. D **8**, 859 (1973) (see Fig. 8).

[13]A. Klar and J. Hüfner, Phys. Rev. D **31**, 491 (1985).

[14]C. De Marzo *et al.*, Phys. Rev. D **26**, 1019 (1982); **29**, 363 (1984); **29**, 2476 (1984).

[15]L. D. Landau, Izv. Akad. Nauk SSSR, Ser. Fiz. **17**, 51 (1953); *Collected Papers of L. D. Landau,* edited by D. Ter Haar (Pergamon, Oxford, 1965), p. 569. For the latest developments in this model, see E. L. Feinberg, Z. Phys. C **38**, 229 (1988), and for applications of the Hanbury-Brown and Twiss method see Y. Hama and Sandra S. Padula, Phys. Rev. D **37**, 3237 (1988).

[16]E. V. Shuryak, Jad. Fiz. USSR **16**, 395 (1972).

[17]S. Pokorski and L. Van Hove, Acta Phys. Pol. **B5**, 229 (1974).

[18]L. Van Hove and S. Pokorski, Nucl. Phys. **B86**, 243 (1975).

[19]P. Carruthers and Minh Duong-Van, Phys. Rev. D **28**, 130 (1983).

[20]G. N. Fowler, E. M. Friedlander, R. M. Weiner, and G. Wilk, Phys. Rev. D **57**, 2119 (1986).

[21]A. Krzywicki, lectures at the International Summer Institute for Theoretical Physics, Centre for Interdisciplinary Research (ZiF), Bielefeld, 1976, Report LPTPE 76/25, 1976 (unpublished).

[22]J. Kapusta, S. Pratt, L. McLerran, and H. von Gersdorff, Phys. Lett. **163B**, 252 (1985).

[23]H. von Gersdorff, Nucl. Phys. **A461**, 251c, (1987).

[24]M. Moravcsik and M. Teper, Phys. Rev. D **16**, 1593 (1977).

[25]K. Kajantie and L. McLerran, Phys. Lett. **119B**, 203 (1982).

[26]L. P. Csernai, M. Gong, and D. Strottman, University of Bergen, Report No. 196, 1988 (unpublished).

[27]J. Stachel and P. Braun-Munzinger, Phys. Lett. B **216**, 1 (1989).

[28]B. Andersson *et al.*, Nucl. Phys. **B281**, 289 (1987); G. Gustafson, University of Lund Report LU-TP-87-17, 1987 (unpublished); B. Nilsson-Almquist and E. Stenlund, Comput. Phys. Commun. **43**, 387 (1987).

[29]K. Werner, Z. Phys. C **38**, 193 (1988).

[30]M. Basile *et al.*, Nuovo Cimento **39A**, 441 (1977).

[31]J. Ranft, Proceedings of the 5th International Symposium on Many Particle Hadrodynamics, Leipzig, 1974, p. 210.

[32]E. L. Feinberg, Usp. Fiz. Nauk. **139**, 3-52 (1983) [Sov. Phys. Usp. **26(1)**, (1983)].

[33]E. L. Berger, Multi-Particle Production Processes at High Energy, L'ecole de Gif sur Yvette, Tome 1, 1973 (unpublished); Nucl. Phys. **B85**, 61 (1975).

[34]A. Arneodo and G. Plaut, Nucl. Phys. **B107**, 262 (1976); D. Drijard *et al.*, *ibid.* **B155**, 269 (1979); J. L. Bailly *et al.*, NA23, EHS-RCBC Collaboration, Institut fur Experimentalphysik, Innsbruck, Two Particle Correlations in 360 GeV/c PP Interactions, 1987 (unpublished).

[35]W. Bell *et al.*, Z. Phys. C **22**, 109 (1984).

[36]P. V. Ruuskanen and D. Seibert, Phys. Lett. B **213**, 227 (1988).

[37]A. Bialas and R. Peschanski, Nucl. Phys. **B273**, 703 (1986).

[38]J. Dias de Deus, Phys. Lett. B **194**, 297 (1987).

[39]R. Holynski *et al.*, KLM Collaboration, Phys. Rev. Lett. **62**, 733 (1989).

[40]C. Quigg, P. Pirila, and G. H. Thomas, Phys. Rev. Lett. **34**, 290 (1975).

[41]D. R. Snider, Phys. Rev. D **11**, 140 (1975).

[42]J. I. Kapusta, Phys. Lett. **143B**, 233 (1984).

[43]R. K. Shivpuri and Chandra Gupt, Phys. Rev. D **15**, 3332 (1977); **17**, 1778 (1978); **27**, 140 (1987); L. M. Barbier *et al.*, *ibid.* **37**, 1113 (1988).

[44]W. Thome *et al.*, (ISR data) Nucl. Phys. **B129**, 365 (1977).

[45]W. R. Press, B. P. Flannery, S. A. Teukolsky, and W. T. Vetterling, *Numerical Recipies* (Cambridge University Press, Cambridge, England, 1986), pp. 191–203.

[46]W. Bell *et al.*, CERN Report No. CERN-EP/85-188, 1985 (unpublished).

[47]T. Abbott *et al.*, E802 Collaboration, Phys. Lett. B **197**, 285 (1987). For a recent review see M. J. Tannenbaum, Nucl. Phys. **A488**, 555c (1988), and S. Nagamiya, Columbia University Report No. 1390, 1988 (unpublished).

[48]P. Braun-Munzinger *et al.*, E814 Collaboration, Z. Phys. C **38**, 45 (1988), and Refs. 5 and 6.

[49]M. Gyulassy, Z. Phys. C **38**, 361 (1988).